ACS Sustainable Chemistry & Engineering

pubs.acs.org/journal/ascecg

Research Article

Revealing the Photophysical Mechanism of *N,N′*-Diphenyl-aniline Based Sensitizers with the D−D−π−A Framework: Theoretical Insights

Juganta K. Roy, Supratik Kar, and Jerzy Leszczynski*

Cite This: *ACS Sustainable Chem. Eng.* 2020, 8, 13328−13341

Read Online

ACCESS | Metrics & More | Article Recommendations | Supporting Information

ABSTRACT: The D−D−π−A framework based dyes are competent for lowering the aggregation and reducing the charge recombination inherently due to their 3D structures. Seven D−D−π−A-based *N,N′*-diphenyl-aniline (NNdPA) dyes are designed and investigated using cluster and periodic density functional theory (DFT) approaches to evaluate their prospect of application in the future dye-sensitized solar cells (DSSCs). The critical parameters related to short-circuit photocurrent density (J_{SC}) and open-circuit voltage (V_{OC}) of the considered dyes such as the driving force of electron injection (ΔG_{Inject}), the spontaneity of dye regeneration (ΔG_{Reg}), the exciton binding synergy (E_b), the charge transfer length (d_{CT}), the reorganization energy (λ_{Total}), the shift of the conduction band of TiO_2 (ΔE_{CB}), the projected density of states (PDOS), and the chemical reactivity parameters were computed. Computed results implied that the fused π-conjugation bridge, along with the benzothiadiazole (BTD) unit, improves the absorption spectrum and charge separation. Also, incorporation of the benzene ring lowers λ_{Total} with balancing its counterparts' reorganization energy. Considering the dye characteristics after electron injection, NNdPA04 with large Stokes shift would possess the most stable excited state due to longer excited state lifetime, τ_e, with the lowest driving force between excited state oxidation potential and conduction band minimum of TiO_2. We found that the presence of the benzene ring in the fused π-conjugation unit increases the light harvesting by shifting the UV−vis spectrum to a longer wavelength. The values of ΔE_{CB} and ΔG_{Reg} suggest that the NNdPA04 and NNdPA10 would be able to suppress the charge recombination and thus enhance V_{OC} of NNdPA-based dyes. The outcomes inferred that the designed NNdPA04 dye could be the lead candidate for the photoefficient NNdPA-based DSSCs. Our work also provides a rational insight into designing the D−D−π−A dyes with a fused π-conjugation.

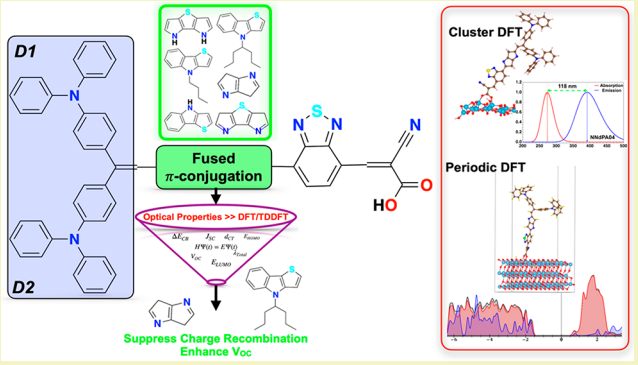

KEYWORDS: *DSSCs, Charge recombination, Fused π-conjugation, Organic dyes, DFT*

INTRODUCTION

The continuous combustion of fossil fuels cannot meet the trajectories toward the achievement of sustainable energy supply. The drive to boost up the use of renewable energy forced the scientific community to design efficient photovoltaics (PVs) technology for harvesting more sunlight.[1] Dye-sensitized solar cells (DSSCs) are affirming to convert solar light to electricity cheaply, compared to most conventional efficient silicon solar cells.[2,3] However, currently DSSCs reached an efficiency of 13.6% using organic triazatruxene dye sensitizers, and there is plentiful room for further improvements of DSSCs.[4] The tunable nature of the sensitizers in dye-sensitized renewable energy areas has created a significant push in research efforts for sensitizer design. Among organic dye sensitizers, the novel and most exploited architectures represent a donor (D) and acceptor (A) motif, i.e., D−π−A, due to its extensive flexibility, efficient push−pull system which is responsible for a better intramolecular charge transfer (ICT) phenomenon, and separation on photoexcitation.[5,6] The ICT band of D−π−A can be shifted to the longer wavelength by (i) enhancing the electron-donating capability of the donor or π-spacer; (ii) improving acceptors' ability for electron withdrawn; and (iii) changing the length and shape of the π-spacer.[7−10] Significant molecular modification approaches such as D−A−π−A[11−13] and D−D−π−A[14−16] architecture based efficient sensitizers have been designed and synthesized, resulting in a higher photoconversion efficiency (PCE) of DSSCs.

Received: June 1, 2020
Revised: July 24, 2020
Published: August 10, 2020

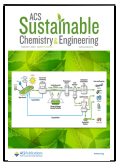

The introduction of the second donor moiety to the D−π−A architecture to form D−D−π−A not only affects the electron donating ability but also improves photochemical and thermal stability.[15,17] Literature suggested that the addition of a double donor moiety in the aromatic amine can also shift the absorption band to the longer wavelengths.[18] Jiang et al. incorporated indoline into a coumarin donor, which improves the antiaggregation ability, V_{OC}, and accordingly improved photovoltaic performance.[19] Estrella and co-workers, theoretically, showed that N-annulated perylene enhanced the dye-to-semiconductor charge transfer mechanism.[20] Hence, the judicious choice of electron-donor pair units in the design of the sensitizer can improve the light harvesting, charge separation, and overall efficiency of the DSSCs.[21] However, the length, symmetry, and rigidity of the π-conjugation spacers play a crucial role in the ICT properties. For instance, long π-conjugation segments between the D and the A groups renders elongated and rod-like structures, which may cause unwanted molecular aggregation of the molecules.[18,22] In DSSCs, two or three ring fused π linkers have been reported in the literature such as thienopyrrole[23] (TP), thieno[2,3-]indole[24] (TI), and pyrrolo[3,2-*b*]pyrrole (PP)[5]. In recent years, researchers have been inspired by polymer PV materials such as benzothiadiazole (BTD) that represent promising candidates to enhance the photovoltaic properties by electron-withdrawing ability in organic polymer solar cells.[25] The BTD moiety improves the charge separation properties due to its narrow bandgap and acts as an electron trap.

In our previous study, we designed 10 new *N*,*N*′-diphenylaniline (NNdPA) dyes explicit to iodine electrolyte, based on the developed quantitative structure−property relationship (QSPR) model. Subsequently, we screened all the designed dyes based on the essential electrochemical properties with the use of quantum chemical calculations. Out of 10, 7 lead dyes have the D−D−π−A framework, and they were characterized by the encouraging PCE values.[26] Our designed D−D−π−A sensitizers encompass: (1) a donor that consists of two NNdPA units connected by an ethylene unit, (2) the rigid π-spacer composed of two or three ring fused conjugation, and (3) a BTD unit as a coacceptor or π-spacer and cyanoacrylic acid (CAA) as an acceptor. We believe our designed NNdPA dyes will be potential candidates for DSSCs to increase the PCE value by suppressing the charge recombination and increasing the electron injection.

Under this background, in the current work, we have performed in detail an investigation of the photophysical mechanism for the new designed isolated dyes and the interface of adsorbed dyes on the TiO_2 surface. Computational approaches were used to calculate different cluster models to provide a meaningful explanation of the local properties of the TiO_2.[27,28] For instance, many theoretical studies considered different sizes of cluster models to gain details related to various organic dyes. Different sizes of TiO_2 clusters such as $(TiO_2)_{16}$,[29] $(TiO_2)_{38}$,[30] and $(TiO_2)_6$[31] have been reported to be used for the study of a variety of dye classes. Multiscale simulation approaches[32] and nonadiabatic molecular dynamics simulation[33] have also been implemented to study optoelectronic properties of isolated T-shaped organic dyes and indoline dyes, respectively. Based on the results reported in the literature,[29,34] we modeled our dye@TiO_2 complex using a small $(TiO_2)_{16}$ cluster to simulate the TiO_2 (101) surface.

In this context, computational investigations focused on the density functional theory (DFT) combined with the time-dependent DFT (TD-DFT) were performed to predict the electronic structure along with the critical parameters that govern the fundamental characteristics of the solar cell, such as the short-circuit photocurrent density (J_{SC}) and the open-current voltage (V_{OC}). All critical parameters including light absorption spectra for the panchromatic region, electron injection, charge recombination, shift of the conduction band (CB) edge, ICT, exciton binding energy, as well as excited state lifetime, and photostability of the dye−cluster complex, were computed. Introspection of a complete analysis of the obtained results will reveal that the new efficient NNdPA dye sensitizers for DSSCs attain higher photo-electron conversion efficiency due to enhanced charge transfer mechanisms and could be used for future applications.

COMPUTATIONAL DETAILS

The overall efficiency of phototo-electron conversion in DSSCs is determined by the integral of short-circuit photocurrent density (J_{SC}), open−circuit photovoltage (V_{OC}), fill factor (FF), and incident solar power on the cell:[35]

$$\eta = FF\frac{J_{SC}V_{OC}}{P_{IN}} \times 100\% \tag{1}$$

The J_{SC} depends on the absorption coefficient of the dye and the interaction between the dye and the nanocrystalline TiO_2 surface. It can be computed by the following equation:

$$J_{SC} = \int_{\lambda} LHE(\lambda)\Phi_{inject}\eta_{collect}\, d\lambda \tag{2}$$

where LHE is light-harvesting efficiency at wavelength λ, Φ_{inject} is the quantum yield for the electron injection efficiency, and $\eta_{collect}$ is the charge collection efficiency which only depends on the architecture of DSSCs. In contrast, other parameters strongly depend on the structural and quantum phenomenon of the dye. Katoh et al.[36] related the injection efficiency to the free energy change for the electron injection (ΔG_{inject}) that can be defined through the following equation:

$$\Delta G_{inject} = E_{ox}^{dye^*} - E_{CB}^{TiO_2} \tag{3}$$

where E_{ox}^{dye}* is the oxidation potential of the dye in the excited state and $E_{CB}^{TiO_2}$ is the reduction potential of the conduction band of semiconductor (TiO_2). The E_{ox}^{dye}* can be computed by subtracting absorption energy associated with the maximum wavelength (λ_{max}) from the ground state oxidation potential (E_{ox}^{dye}) of the dye that is equal to the negative value of the HOMO energy of the isolated dyes.

$$E_{ox}^{dye^*} = E_{ox}^{dye} - \lambda_{max} \tag{4}$$

Also, the driving force for dye regeneration (ΔG_{regn}) can be calculated via the following expression:

$$\Delta G_{regn} = E^{redox} - E_{ox}^{dye} \tag{5}$$

The DFT and TD-DFT frameworks were used to optimize and calculate the different properties of isolated NNdPA dyes with B3LYP and CAM-B3LYP functionals using the 6-311G(d,p) basis set in the Gaussian09 package.[37] We also performed frequency calculations to confirm that the obtained structures have no imaginary frequency. Simulated UV−visible absorption spectra were obtained with the use of the CAB3LYP/6-311G(d,p) level of theory by applying the conductor-like polarized continuum model (C-PCM) of the acetonitrile solvent. Emission spectra of the isolated dyes were measured in the gas phase to see the trend of fluorescence properties. Multiwfn 3.3.9 code was used to calculate ICT parameters and visualize centroids.[38]

We used two different approaches to describe the TiO_2 semiconductor: (a) the cluster model and (b) the periodic model. The cluster model allows the convenient use of hybrid exchange-

https://dx.doi.org/10.1021/acssuschemeng.0c04061
ACS Sustainable Chem. Eng. 2020, 8, 13328−13341

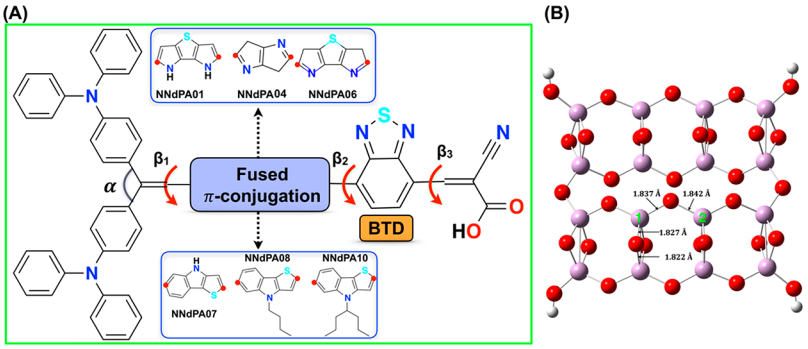

Figure 1. (A) General molecular structure of the designed NNdPA dyes along with its structural features (dihedral angle, conjugation constituents). Red dots in the fused π-conjugation fragments indicating the linkage position and (B) optimized $(TiO_2)_{16}$ cluster with the (101) crystal facets and notable bond lengths. It is noted that NNdPA01 does not containa BTD unit and NNdPA03 does not have any fused π-conjugation.

correlation functionals along with continuum solvation models. However, it is not suitable for the global model description. On the other hand, periodic formalism provides for a more precise description of the surface properties, which is free from finite-size effects. For both cases, we considered bridged bidentate (BB) anchoring which is the most stable among all other binding modes.[34,39,40]

In cluster DFT, geometry optimizations were done in the gas and acetonitrile solvent phases. We use stoichiometric $(TiO_2)_{16}$ clusters which have been demonstrated to reproduce to a good degree of accuracy the DOS of bulk anatase. In all cases, our TiO_2 models expose the majority of the (101) surfaces.

Periodic DFT calculations were performed using the Vienna ab initio Simulation Package (VASP)[41−43] under generalized gradient approximation (GGA) using the Perdew−Burke−Ernzerhof (PBE) exchange-correlation functional with Hubbard onsite Coulomb repulsion term;[44] we named the method DFT+U. Based on our previous work,[45] we choose an effective U value of 3.5 eV which gives a reliable description of the bandgap. In the dye@TiO_2 system, we describe C $1s^2$, O $1s^2$, N $1s^2$, Ti-[Ne] $3s^2$, and S-[Ne] core electrons with the projector augmented wave (PAW) pseudopotentials.[46] The cutoff energy of the plane-wave basis set was 400 eV with a Γ centered Monkhorst−Pack grid of 0.03 $Å^{-1}$ separation. The total energy converged to <1 meV/atom. All the structures considered in this study were fully relaxed until all the forces and energies were less than 0.03 eV/Å and 10^{-6} eV/atom, respectively. The anatase TiO_2(101) supercell was modeled with three O−Ti−O layers (288 atoms) along the z-direction, and the dye molecules were adsorbed on one side of the slab with a 15 Å vacuum from the top of the molecules.

RESULTS AND DISCUSSION

Molecular Structures of NNdPA Dyes. Structural attributes such as the dihedral angle, interplanar angle, and bond length of the different units of the sensitizer directly affect the properties in the gas and solvent phases. Different attributes and their positions are illustrated in Figure 1, and their values are listed in Table 1. The interplanar angle (π) between two donor units can shield the semiconductor from an oxidized electrolyte to suppress the unfavorable recombination process.[5] The value of π is almost the same for all of the investigated dyes confirming that the use of different fused π-spacers has little influence on donor orientations.[39] The dihedral angle, β_1, for NNdPA06 is the lowest while NNdPA07, NNdPA08, and NNdPA10 have the higher values. Steric hindrance arising from the benzene rings fused with a π-spacer might be the reason for the more substantial β_1 value. β_2 represents the dihedral angle between the fused conjugation and the coacceptor unit, BTD. The values of β_3, which represent the dihedral angle between the BTD unit and cyanoacrylic acid (A), range from 0.40° to 26.27°. NNdPA03 is characterized by the higher value of β_3 due to the absence of a fused conjugation unit while NNdPA04 has a planar structure. It is imperative to maintain the planarity for the easy flow of charge transfer from the donor to the acceptor unit. The planarity of $\pi-A$ is perturbed with the increase (or type) of the fused conjugation unit. The optimized geometry of the isolated NNdPA dyes is depicted in Figure S1 (see the Supporting Information).

Table 1. Structural Attributes of the NNdPA Dyes[a]

dye	π	β_1	β_2	β_3
NNdPA01	117.08	29.80	NA	NA
NNdPA03	117.28	29.45	NA	26.27
NNdPA04	117.46	29.70	1.06	0.40
NNdPA06	116.86	25.60	1.22	1.48
NNdPA07	116.76	33.12	1.78	3.08
NNdPA08	116.94	32.35	2.86	5.34
NNdPA10	116.92	32.33	3.21	4.98

[a]All the angles are in degrees.

Electronic Properties of the Isolated Dyes. The intrinsic electronic structures of the dyes such as frontier molecular orbital (FMO) distribution and their energetics potentially affect the electronic transfer and excitation characteristics of the dyes. Figure 2 depicts the important FMOs including the highest occupied molecular orbitals (HOMOs) and lowest unoccupied molecular orbitals (LUMOs) of the isolated dyes in the acetonitrile solvent. FMO can be used to evaluate the intermolecular charge transfer and charge transfer state. The HOMOs (Figure 2) of all the investigated dyes are distributed on the donor and π-bridge (except NNdPA01 and NNdPA03), while the LUMOs are primarily localized on the π-bridge and acceptor units. NNdPA01 and NNdPA03 are an exception due to the number of acceptor units and the length of the conjugation fragment, respectively. Also, these two dyes are distinctly different from the other five dyes in the structure because NNdPA01 lacking a BTD unit and NNdPA03 do not have any rigid conjugation moieties. It is well-known that π-bridges are responsible for providing a route for charge transfer and redistribution in $D-\pi-A$ architecture dyes.[47] In the case of NNdPA06, the first excitation dominated by the HOMO−2 to LUMO transition, while all the dyes possess a HOMO to LUMO transition (Table 2). NNdPA04, NNdPA06, NNdPA07, NNdPA08, and

https://dx.doi.org/10.1021/acssuschemeng.0c04061
ACS Sustainable Chem. Eng. 2020, 8, 13328−13341

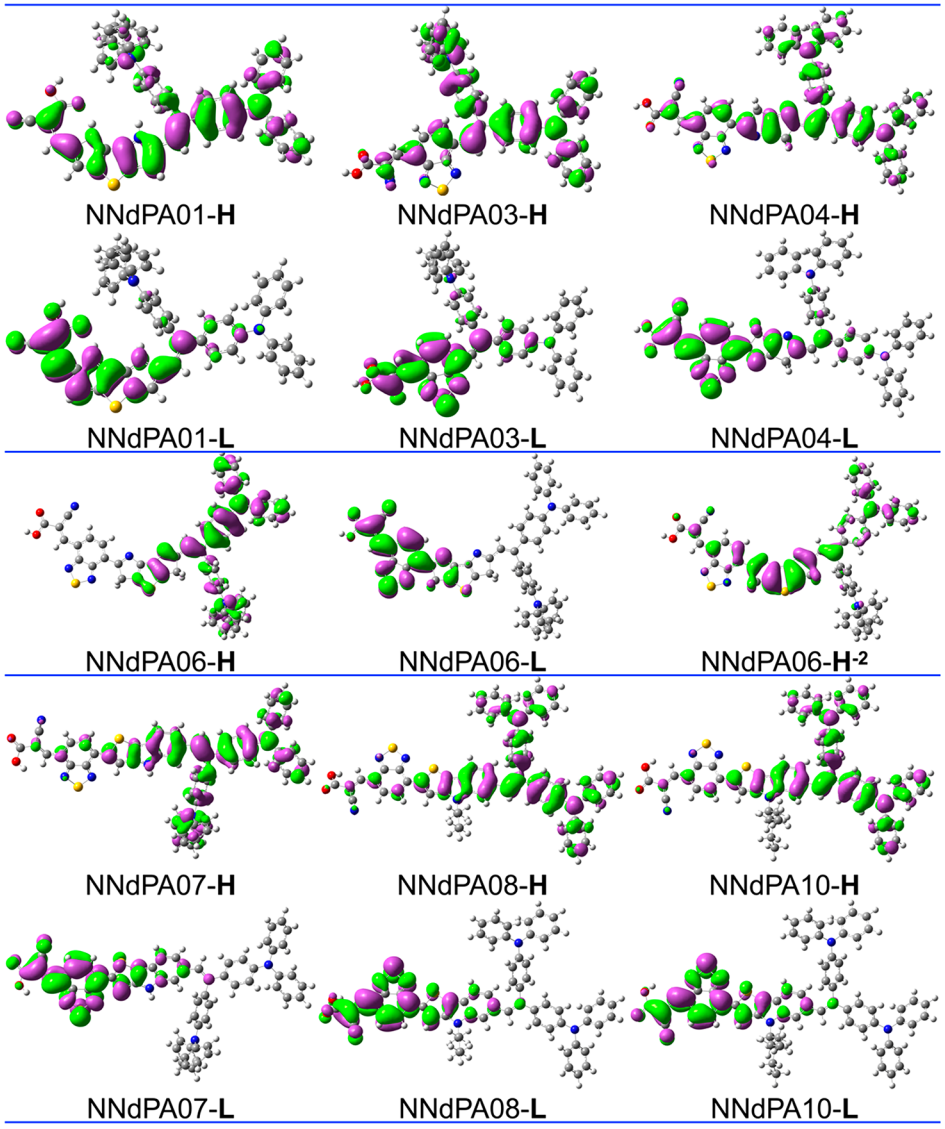

Figure 2. Electron density distribution of the important molecular orbitals of the isolated dyes in acetonitrile solvent. H, H^{-2}, and L represent HOMO, HOMO−2, and LUMO. In all the cases the isovalue is set to 0.02.

NNdPA10 show effective charge separation due to the introduction of different electronegative heteroatoms in the same ring, which enhances the push−pull effect of the dyes by effectively promoting the intermolecular electron transfer.[12]

Different approaches have been reported to include double donor in sensitizers.[14,15] Hagberg et al. studied single (D9) and double donor (D11) based sensitizers and found that both possess almost similar solution-phase optical energy gaps. However, the authors also mentioned that although D11 is promising to increase the V_{OC}, D9 is a winner dye for higher photoconversion efficiency in the solid-state solar cells. Besides, D11 possessed excellent photochemical and thermal stability along with higher photoconversion efficiency in the liquid cell to compare to solid-state solar cells. To take account of the effect of double donors on geometry and electronic properties of the designed NNdPA dyes, we followed a similar procedure for the single donor analogues (see Figure S1). We observed that the former one pushed the HOMO energy level into the range of 30 to 110 meV (Table S1), which is crucial as the HOMO in DSSCs always suffers from lower energy. Moreover, we implemented our computational methodology for D9 and D11 to benchmark our methods and designed dyes. The results revealed that the HOMO energy level of D11 is 0.32 eV higher than that of D9, which reduces the E_{gap} by 0.2 eV. In contrast, experimental results show no change in the optical energy gap, suggesting that there might be other factors responsible for the deviation in both experimental and theoretical results.

Energy level alignment is the most critical factor for any efficient solar cells. According to the DSSC's working principle, the HOMO and LUMO energy levels of dyes should be higher than the CB minima of TiO_2 (−4.0 eV) to maintain the efficient electron injection and lower the redox potential of the iodine electrolytes (−4.8 eV) to ensure the dye regeneration, respectively. Figure 3 outlines the orbital energy level of the investigated dyes and shows that they comply with the basic requirements of DSSCs. The HOMO−LUMO energy gap (E_{gap}) governs the photon absorption by any individual dye and thus changes the shape of the UV−vis spectrum. Lower E_{gap} eases the transition of molecules from the ground state to an excited state and shifts the absorption peak to the higher wavelengths.

https://dx.doi.org/10.1021/acssuschemeng.0c04061
ACS Sustainable Chem. Eng. 2020, 8, 13328−13341

Table 2. Computed TD-DFT Excitation Energies (eV, nm), Oscillator Strengths (f), Compositions in Terms of Molecular Orbital Contributions, and Their Character of the Transition of NNdPA Isolated Dyes in Acetonitrile Solvent Predicted with the Use of the B3LYP/6-311G(d,p)/CPCM Level of Theory

NNdPA dye	E (eV) [λ_{max} (nm)]	f	major contribution	dominant transition[a]
01	2.43 [510.34]	1.6357	$H \rightarrow L$ (78.03%)	ICT + (π,π^*)
	3.42 [362.51]	0.7927	$H \rightarrow L^{+1}$ (40.20%), $H^{-2} \rightarrow L$ (32.72%)	(π,π^*)
03	2.21 [559.95]	1.2496	$H \rightarrow L$ (78.49%), $H^{-2} \rightarrow L$ (17.65%)	ICT + (π,π^*)
	4.18 [296.49]	0.7541	$H^{-1} \rightarrow L^{+2}$ (33.64%), $H \rightarrow L^{+4}$ (30.96%)	(π,π^*)
	2.96 [419.18]	0.3686	$H^{-2} \rightarrow L$ (90.35%)	(π,π^*)
04	1.69 [732.91]	1.7472	$H \rightarrow L$ (77.83%), $H^{-2} \rightarrow L$ (13.47%)	ICT + (π,π^*)
	2.93 [423.87]	0.3504	$H^{-1} \rightarrow L$ (66.47%), $H \rightarrow L^{+1}$ (13.87%)	(π,π^*)
	3.69 [336.33]	0.3901	$H^{-1} \rightarrow L^{+1}$ (54.21%)	(π,π^*)
06	2.51 [494.96]	1.2233	$H^{-3} \rightarrow L$ (23.02%), $H^{-2} \rightarrow L$ (69.75%)	(π,π^*)
	3.17 [391.65]	1.1349	$H \rightarrow L^{+1}$ (75.17%)	(π,π^*)
	2.88 [429.93]	0.1924	$H^{-3} \rightarrow L$ (10.77%), $H \rightarrow L$ (74.53%)	ICT + (π,π^*)
07	2.33 [610.08]	1.7842	$H \rightarrow L$ (51.59%), $H^{-2} \rightarrow L$ (38.88%)	ICT + (π,π^*)
	3.30 [375.36]	0.2016	$H^{-1} \rightarrow L$ (79.60%)	(π,π^*)
	3.78 [327.98]	0.5987	$H \rightarrow L^{+2}$ (55.13%)	(π,π^*)
08	1.99 [623.68]	1.8773	$H \rightarrow L$ (54.24%), $H^{-2} \rightarrow L$ (36.38%)	ICT + (π,π^*)
	3.33 [372.42]	0.2292	$H^{-1} \rightarrow L$ (83.46%)	(π,π^*)
10	1.98 [625.22]	1.8708	$H \rightarrow L$ (54.58%), $H^{-2} \rightarrow L$ (35.58%)	ICT + (π,π^*)
	3.49 [355.17]	0.7627	$H \rightarrow L^{+2}$ (57.86%), $H \rightarrow L^{+4}$ (11.57%)	ICT + (π,π^*)

[a] (π,π^*), H^{-n}, and L^{+m} indicate ($\pi \rightarrow \pi^*$), nth HOMO and mth LUMO, respectively. Singlet states are arranged based on OS(f).

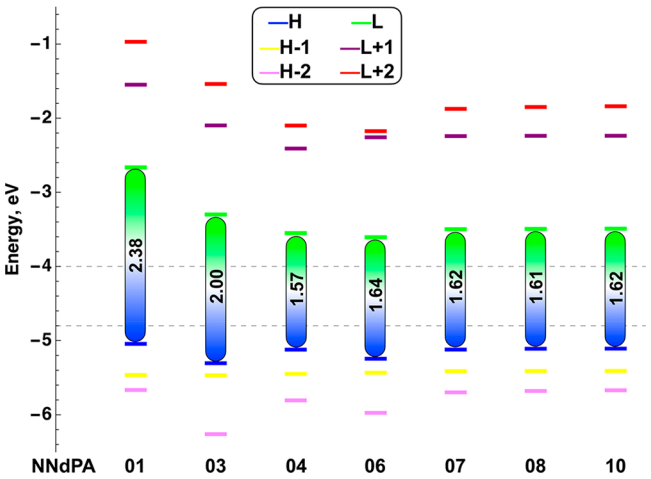

Figure 3. Computed orbital energy (in eV) levels, HL gap along with the CB level of TiO_2 (−4.0 eV), and redox potential of iodine electrolyte (−4.8 eV). H and L represent HOMO and LUMO.

As depicted in Figure 3, E_{gap} values of NNdPA04, NNdPA06, NNdPA07, NNdPA08, and NNdPA10 lie in the range of 1.57 to 1.64 eV, while NNdPA01 and NNdPA03 have a higher band gap compared to the other considered dyes. Because the inclusion of heterocycles increases the planarity of the dye molecule as well as the conjugation length, it helps to lower the E_{gap}. Also, NNdPA01 has the largest E_{gap} among the considered dyes due to the lack of the BTD unit. The BTD unit has been used in organic photovoltaic (OPV) cells[48] as the building block of low-band gap polymers and in metal-free based DSSCs to have good performance.[40,49] We also found that the inclusion of the BTD unit as an internal acceptor in the indoline dyes effectively red-shifted the absorption spectra by reducing the E_{gap}.[34] NNdPA01 and NNdPA06 have relatively large E_{gap} values due to the introduction of more heteroatoms in the π-bridge lead steric hindrance from the nitrogen atoms as well electron rich nitrogen atoms breaking the conjugation in the CT path. Similar phenomena were reported by Liu et al.[47] and Kim et al.[50] in the cases of boron dipyrromethene dye based DSSCs and carbazole based polymer solar cells, respectively. Again, the introduction of heterocycles with an internal acceptor like BTD may be a better strategy to promote electron excitation, thereby facilitating the light absorption of molecules at longer wavelengths. However, Haid et al.[10] reported that the use of a π-spacer in between the BTD unit and CAA boosts the efficiency of the solar cell as the absence of the π-spacer increases the rate of back-electron transfer. Authors also mentioned that the cationic state of the latter one is more stable than that of the former one and the use of the π-spacer hinders the conjugation continuity by changing the dihedral angle. DFT computed results were confirmed with the use of ultrafast spectroscopy. By taking this observation, we have checked our designed dyes with the incorporation of a benzene unit between BTD and CAA. We have analyzed the orbital energies of the neutral state (HOMO) and singly occupied molecular orbital (SOMO) energies of the cationic state of both sets of dyes (Table S5), and we observe that the SOMO values of BTD-π-CAA are higher than the BTD-CAA for most of the dyes except NNdPA08, whereas there is no significant difference in HOMO energies. This result revealed that the cationic state of the BTD-CAA based NNdPA dyes is more stable than that of the BTD-π-CAA based dyes. The simulated UV−vis absorption results for the first excitation energy $S_0 \rightarrow S_1$ of the selected NNdPA dyes are tabulated in Table S5. Our reported results and the literature suggest that the designed NNdPA dyes show better light-harvesting abilities compared to the BTD-π-CAA analogues. The designed NNdPA dyes are potential candidates in conjunction with the TiO_2, where efficiency might suffer from a trade-off between the photocurrent and the photovoltage. However, Lin et al.[51] used BTD directly connected to the CAA groups in conjunction with the ZnO photoanode instead of TiO_2 with improved conversion efficiency from 4.02% to 5.82%.

The light absorption behavior of the sensitizer is a crucial factor in understanding and evaluating its photophysical properties. DSSCs with a high PCE require that the sensitizer's absorption spectra should match as close as possible the solar spectrum to absorb maximum solar radiation. The simulated UV−vis absorption spectra of the isolated dye and dye@TiO_2 complexes in acetonitrile solvent are presented in Figure 4. Maximum absorption wavelengths (λ_{max}), oscillator strengths (f), and transition characters for the dyes are collected in

https://dx.doi.org/10.1021/acssuschemeng.0c04061
ACS Sustainable Chem. Eng. 2020, 8, 13328−13341

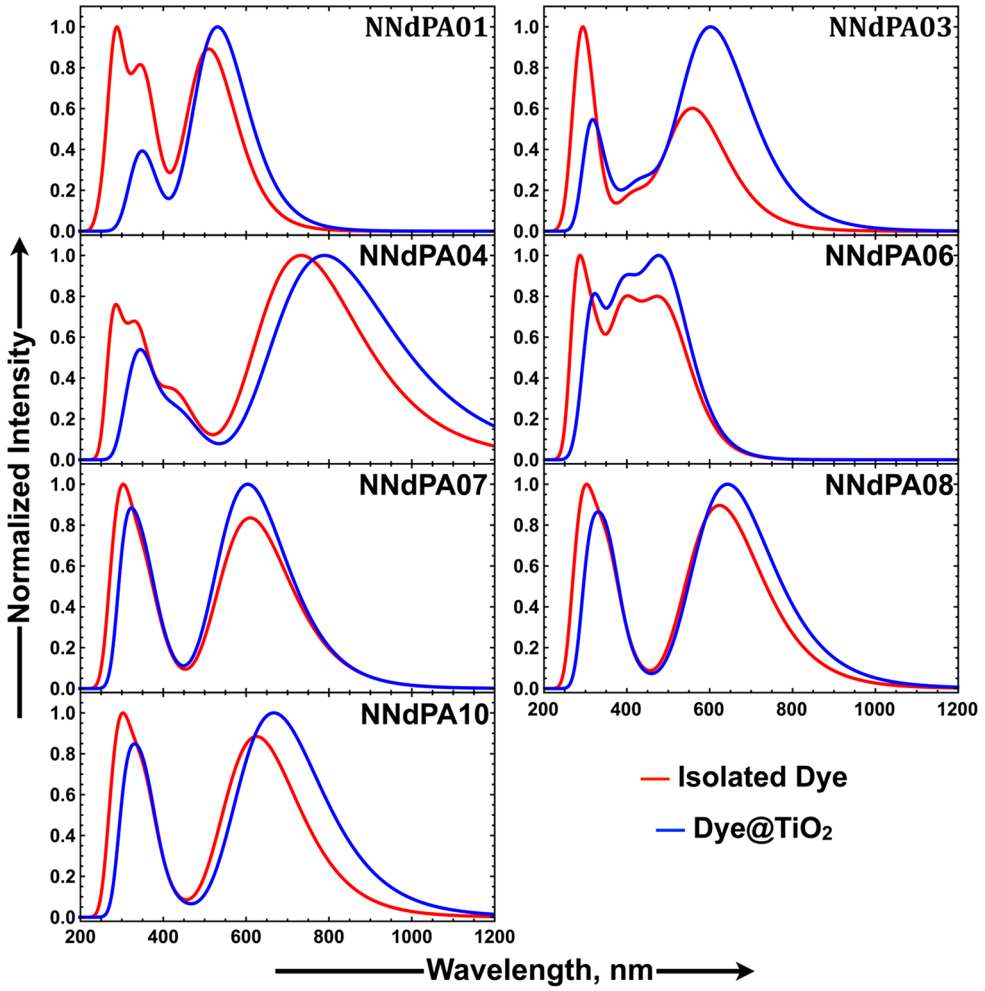

Figure 4. UV−vis absorption spectra of the isolated NNdPA dyes and dye@TiO_2 complexes in acetonitrile solvent simulated at the TDDFT/CPCM/CAM-B3LYP/6-311G(d,p) level of theory. For Ti only the LANL2DZ basis set was used.

Table 3. Bond Distances (Å) between Ti of TiO_2 and O Atoms of (−COOH) NNdPA Dyes and Adsorption Energy (in eV) of NNdPA Dyes Considering Both the Cluster and Periodic Model[a]

	cluster DFT		periodic DFT	
dye	E_{ads}, eV	d_{Ti-O},[b] Å	E_{ads}, eV	d_{Ti-O},[b] Å
NNdPA01	−0.92	2.04	−2.72	2.08
NNdPA03	−1.01	2.04	−3.34	2.09
NNdPA04	−1.17	2.01	−3.06	2.11
NNdPA06	−1.18	2.02	−3.18	2.22
NNdPA07	−1.07	2.07	−3.10	2.21
NNdPA08	−1.22	2.07	−3.17	2.22
NNdPA10	−1.59	2.02	−3.21	2.19

[a]For clusters, DFT calculations were performed with acetonitrile solvent. [b]d_{Ti-O} = Average bond distance.

Table 2. The spectra of these dyes have two distinct absorption bands in the UV and visible regions.

The absorption at shorter wavelengths ranged from 200 to 400 nm can be described by $\pi-\pi^*$ electronic transitions by NNdPA dyes, and the longer wavelengths ranging between 400 to 1200 nm (except NNdPA06) can be categorized by the intramolecular charge transfer phenomenon from the donor unit to the acceptor unit. The absorption peaks at 400 to 1200 nm can be assigned to the $S_0 \rightarrow S_1$ transition (for NNdPA06 $S_0 \rightarrow S_2$). It is important to mention that λ_{max} of all the dyes is red-shifted due to the incorporation of the BTD unit compared to NNdPA01, except NNdPA06 and their spectral response ranges are broadened to the near-infrared regions. The lack of a benzene ring in the fused π-conjugation of NNdPA01 and NNdPA06 resulted in a blue-shift as well as a hypochromic shift compared to other dyes. The NNdPA04 has the highest λ_{max} with broader spectrum near-infrared regions which confirm the harvesting of the maximum photon. Again, the NNdPA04 might be benefited from the pyrrole unit as fused conjugation with fewer heteroatoms, although NNdPA07, NNdPA08, and NNdPA10 have similar response ranges, but the behavior after the adsorption has changed. The main configurations are dominated by the electronic transition between $H(H^{-2})$ to L for which the spatial separation of the molecular orbital means that there is an intramolecular charge transfer taking place upon excitation. Judicious choice of fused conjugation units in conjunction with the BTD unit will improve the light-harvesting ability, charge transfer phenomenon, and ultimately the higher PCE.

Once the dyes are adsorbed on the surface of TiO_2, their absorption spectra will be affected accordingly. The computed absorption spectra of dye@TiO_2 complexes might reasonably approximate the spectra in the cell devices. In comparison to the isolated dyes, all the dye@TiO_2 complexes (except NNdPA06 and NNdPA07) are red-shifted (see Table S4),

https://dx.doi.org/10.1021/acssuschemeng.0c04061
ACS Sustainable Chem. Eng. 2020, 8, 13328−13341

Table 4. Photophysical Properties, Reorganization Energies, and Excited State Lifetimes of Isolated NNdPA Dyes in Acetonitrile Solvent Predicted DFT/CPCM/B3LYP/6-311G(d,p) Level of Theory

dye	ΔG_{Inject}	ΔG_{Reg}	λ_h	λ_e	λ_T	q_{CT} (e^-)	d_{CT} (Å)	H (Å)	t (Å)	E_b (eV)	ΔE_{CB}, eV	τ_e (ns)
NNdPA01	−1.16	−9.84	0.28	0.26	0.54	0.70	2.08	1.39	0.69	0.05	0.18	2.38
NNdPA03	−0.73	−10.01	0.11	0.29	0.40	0.74	3.59	1.45	2.14	0.20	0.20	3.78
NNdPA04	−0.42	−9.91	0.25	0.27	0.52	0.75	3.72	1.14	2.58	0.13	0.35	4.56
NNdPA06	−0.94	−10.02	0.42	0.22	0.64	0.85	2.43	1.30	1.13	0.87	0.27	2.30
NNdPA07	−0.64	−9.91	0.23	0.22	0.45	0.86	3.78	1.41	2.37	0.41	0.24	3.13
NNdPA08	−0.62	−9.90	0.25	0.22	0.47	0.90	3.60	1.39	2.21	0.37	0.28	3.10
NNdPA10	−0.61	−9.90	0.25	0.22	0.47	0.93	3.45	1.32	2.13	0.36	0.38	3.14

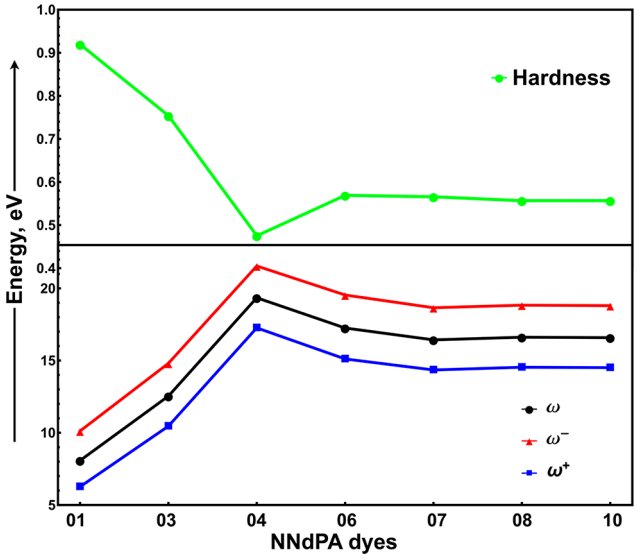

Figure 5. Chemical reactivity parameters such as chemical hardness, electrophilicity (ω), and electron-accepting (ω^+) and electron-donating (ω^-) power of the NNdPA dyes computed at the DFT/B3LYP/6-311G(d,p) level of theory.

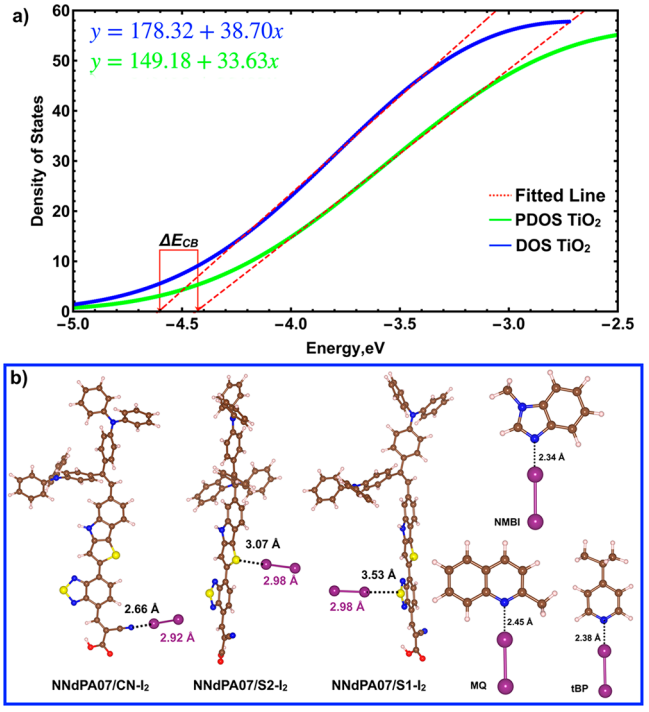

Figure 6. (a) Total DOS plot of the dye adsorbing on the $(TiO_2)_{16}$ cluster and PDOS of NNdPA01 and TiO_2. The inset is a presentation of the approximated ΔE_{CB} derived by linear fitting of PDOS and DOS of TiO_2. (b) Dye−I_2 complex of NNdPA07 with the bond distances of I_2 with the three additives. NMBI: NMN-methylbenzimidazole, MQ: 2-methylquinoline, and tBP: 4-*t*-butylpyridine. Color code: violet (iodine), red (oxygen), brown (carbon), yellow (sulfur), blue (nitrogen), and white (hydrogen).

and higher oscillator strength is observed, which is beneficial to absorption and utilization of more sunlight.[29,34] We believe that the red-shift of the spectra stems from the interaction of the −COOH group and Ti 3d orbitals which can be characterized by the decreased LUMO energy level (see Figure S3). Also, the use of different solvents may predict different absorption behaviors. Some studies showed that the use of a basic solvent with suitable additives can shift the CT transition in the shorter wavelength.[52] The absorptions of NNdPA01, NNdPA03, NNdPA04, NNdPA08, and NNdPA10 complexes are red-shifted by about 21, 42, 57, 20, and 45 nm, respectively.

Adsorption of Dyes on TiO_2. To evaluate the overall performance of NNdPA dyes, we approximate the TiO_2 by the TiO_2 cluster (Cluster DFT) and TiO_2 surface models (Periodic DFT). For this section the TiO_2 cluster and TiO_2 slab will be named as cluster and slab, respectively. For both considered cases, the interaction of the dye with the TiO_2 semiconductor was qualitatively evaluated by the distance between two Ti−O bonds and the adsorption energy (E_{ads}), which can be computed by the relation $E_{ads} = E_{TiO_2+Dye} + E_{TiO_2} + E_{Dye}$. The optimized structure of the dye@cluster complex is depicted in Figure S2 (see Supporting Information). Computed bond distances and adsorption energies are listed in Table 3. A smaller bond length and lower value of E_{ads} confirm the formation of stable complexes and will favor the efficient electron injection from the LUMO of the dye to the CB edge of TiO_2. If the bond length of the Ti−O bond is shorter than 2.05−2.10 Å, dyes interact strongly with the TiO_2 nanoparticle.[53,54] For all the investigated dyes, the average bond length ranges between 2.01 and 2.07 Å. It is fascinating that NNdPA04 has the lowest bond distance with moderate E_{ads} while it shows the largest red-shift (ca. 57 nm) compared to NNdPA01 with *ca.* 789 nm λ_{max}.

Photophysical Properties. In this section, different photophysical properties of isolated NNdPA dyes will be discussed based on the implemented DFT/TD-DFT level of calculations. The estimated properties are tabulated in Table 4.

Intermolecular Charge Transfer (ICT) Characteristics. Light absorption by the sensitizers benefited from the transition of ICT and excited states with significant charge separation properties.[55] We have implemented the comprehensive electron−hole analysis of excitation to get insight into the charge transfer (CT) and ICT phenomenon.[56,57] ICT related indicators like the charge transfer length (d_{CT}) between

https://dx.doi.org/10.1021/acssuschemeng.0c04061
ACS Sustainable Chem. Eng. 2020, 8, 13328−13341

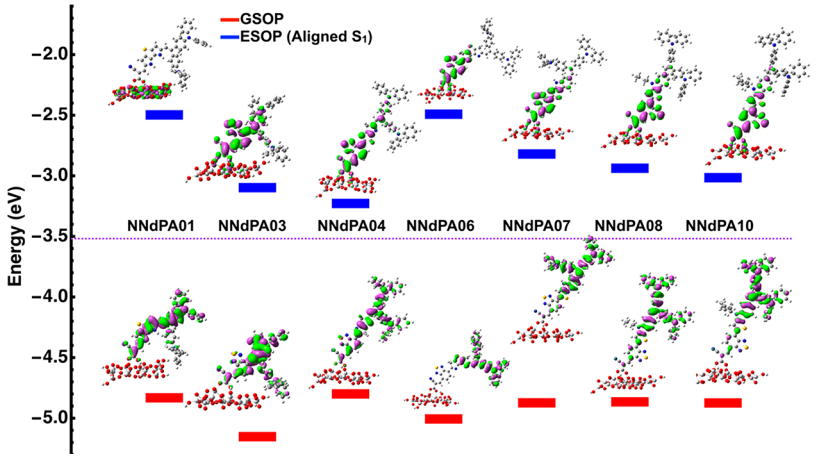

Figure 7. Alignment of the energy of NNdPA dyes@cluster complexes along with the frontier molecular orbitals (HOMO, LUMO) and CB edge of TiO_2 (dotted violet line).

the centroids of the electrons and hole upon excitation, transferred charge (q_{CT}), and H index, which is an overall measure of spatial extension degree of the electron and hole, are computed. Also, the term t can be related to $t = d_{CT} - H$, a reasonable diagnostic index to quantify through the space transitions which denotes a substantial charge separation if it has a positive value. The t index is positive for all of the NNdPA dyes. Considering that CT, for a rod-like system, occurs along the x-axis, H can be express as[57]

$$H = \frac{\sigma^{+x} + \sigma^{-x}}{2} \tag{6}$$

where π is the root-mean-square deviation distance along the x-axis. A larger value of t indicates that the separation is broad between the density increment and the depletion regions. Exciton binding energy (E_b) also affects the ICT process which can be estimated by the energy difference between the electronic and the optical band gap ($|E_b| = E_{gap} - E_{S1}$),[58,59] where E_{S1} is the first singlet excitation energy. We can expect CT effects with substantial separation for all the NNdPA dyes for the $S_0 \rightarrow S_1$ transition corresponding to the maximum absorption peak as d_{CT} is larger than the C−C bond length. For the first transition, an addition of the BTD unit can elongate the CT length comparing to NNdPA01. NNdPA06 shows the smallest length because of the highest number of heteroatoms in the fused π-conjugation unit without a benzene ring. In the case of photoinduced excitation, a more effective charge separation with stronger CT behavior is usually observed in the $S_0 \rightarrow S_1$ transition. Estimated values of d_{CT} and q_{CT} imply that strong ICT is more likely to occur for all the dyes, except NNdPA01 and NNdPA06. An intramolecular electron−hole (exciton) pair will be formed immediately after the ICT, and this process is termed as molecular exciton upon photoexcitation. For the propitious separation of the photo-induced exciton, E_b must be overcome and a smaller value of E_b efficiently promotes exciton dissociation. The computed values of E_b presented in Table 4 indicate that the exciton in the dye NNdPA04 is easier to separate compared to other dyes and the predicted barrier reaches the maximum for NNdPA06. This dye is characterized by the major contribution H to L from $S_0 \rightarrow S_2$. NNdPA01 possesses the lowest E_b without BTD unit which is responsible for lowering the LUMO and enhancing the electron injection to the CBM.

Electron Injection. Marcus semiclassical theory[60] (eq 7) can be used to understand the CT rate by defining electron (λ_e), hole (λ_h), and total reorganization energy (λ_{Total}).

$$k_{ET} = \frac{1}{\sqrt{\lambda_{Total}}} \sqrt{\frac{\pi}{\hbar^2 k_B T}} |V^2| \exp\left\{-\frac{\lambda_{Total}}{4k_B T}\right\} \tag{7}$$

Except for λ_{Total}, all the parameters on the right-hand side of the equation such as k_B (Boltzmann constant) and $\hbar$ (Planks' constant) are constant. Thus, the electron transfer rate constant (k_{ET}) depends only on λ_{Total}, which is a sum of λ_h and λ_e, whose values can be estimated by the eqs[61] 8 and 9, respectively.

$$\lambda_h = (E_0^+ - E_+^+) + (E_+^0 - E_0^0) \tag{8}$$

$$\lambda_e = (E_0^- - E_-^-) + (E_-^0 - E_0^0) \tag{9}$$

where E_0^+ (E_0^-) denotes the energy of the cation (anion) calculated from the optimized structure of the neutral molecule; E_+^+ (E_-^-) is the energy of the cation (anion) calculated from the optimized cation (anion) geometry; E_+^0 (E_-^0) is the energy of the neutral molecule computed from the cationic (anionic) state; and E_0^0 is the energy of a neutral molecule at the ground state.

The rate of CT increases with decreasing λ_{Total}. Therefore, the calculated λ_{Total} is also important for the analysis of the relationship between the electronic structure and the electron injection density (J_{SC}). Accordingly, our discussion focuses predominantly on the reorganization energy, i.e., only the internal reorganization energy is determined in this study, while the impact of the external environment is neglected. From Table 4, one can see that the presence of the benzene ring at the donor side positively affects the electron transfer with lower λ_{Total}, balancing its counterpart reorganization energy. A similar result has been reported for the D−π−A based organic dye in the literature.[62] Furthermore, a counterbalanced transport of holes and electrons is crucial for highly efficient DSSCs; i.e., the LHE increases when the reorganization energies of holes and electrons converge.[63,64] This result shows that the difference between the hole reorganization energy (λ_h) and the electron reorganization energies (λ_e) for NNdPA01, NNdPA03, NNdPA04, NNdPA06, NNdPA07, NNdPA08, and NNdPA10 are 0.02, 0.18, 0.02, 0.20, 0.01, 0.03, and 0.03 eV, respectively.[26] Thus,

https://dx.doi.org/10.1021/acssuschemeng.0c04061
ACS Sustainable Chem. Eng. 2020, 8, 13328−13341

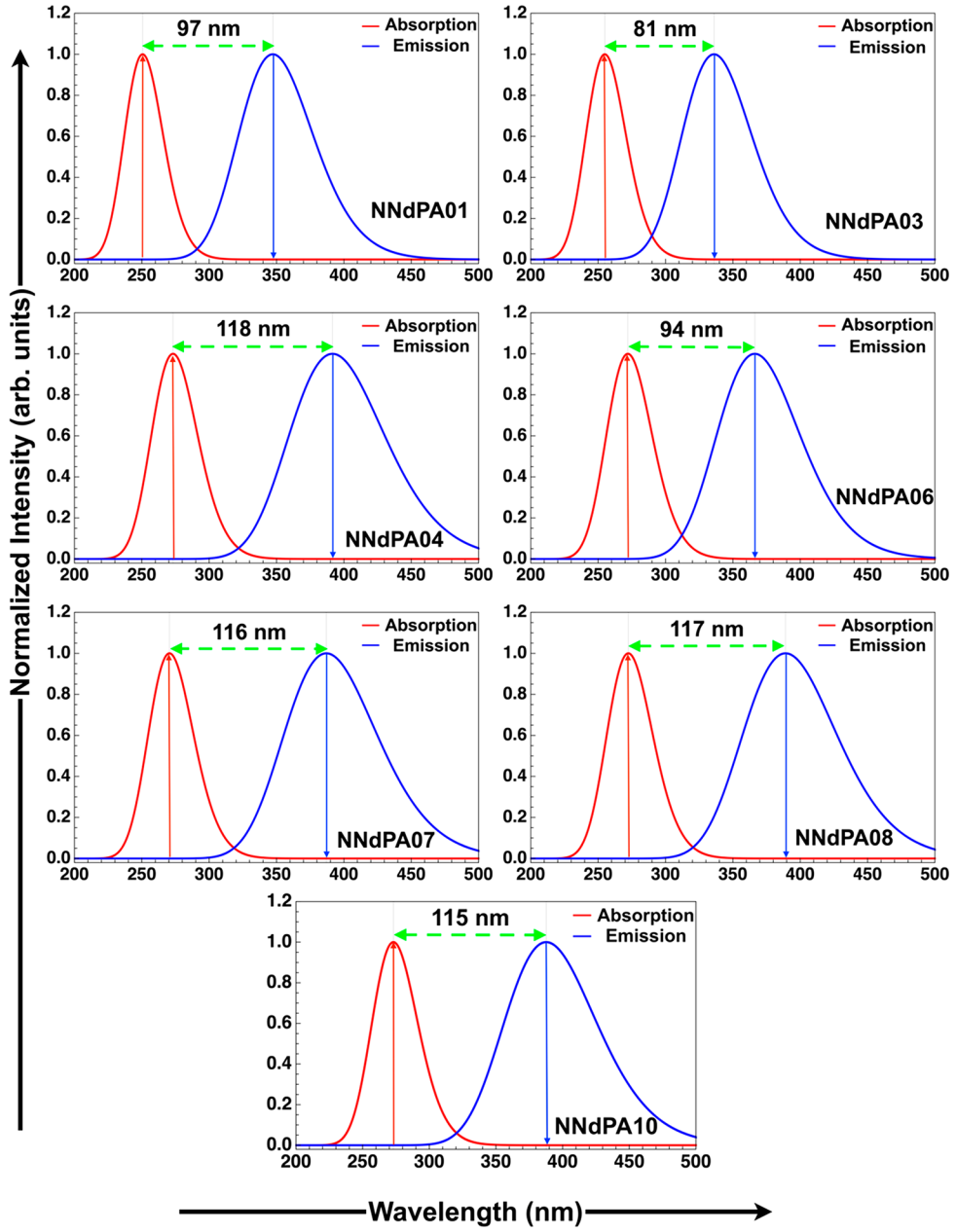

Figure 8. Absorption and emission spectra of the designed dyes in the gas phase along with the Stokes shift computed with the CAM-B3LYP/6-311G(d,p)//B3LYP/6-311G(d,p) level of theory.

Table 5. Calculated Emission Energies (E_{emi}), Emission Peaks (λ_{emi}), Oscillator Strengths (f), and Radiative Lifetimes (τ_f) of the Designed Dyes in the Gas Phase for the $S_0 \leftarrow S_1$ Transition

dye	E_{emi} (eV)	λ_{emi} (nm)	f	τ_f (ns)
NNdPA01	3.57	347.25	0.0107	0.23
NNdPA03	3.69	336.05	0.1969	0.01
NNdPA04	3.17	391.54	0. 0704	0.04
NNdPA06	3.38	366.30	0. 0198	0.14
NNdPA07	3.20	386.96	0. 0779	0.04
NNdPA08	3.19	389.11	0. 1034	0.03
NNdPA10	3.20	387.72	0. 1021	0.03

all the dyes except NNdPA03 and NNdPA06 show considerable counterbalance among the reorganization energies of the electrons and holes.

In DSSCs, the electron injection phenomenon can be elucidated by the CT process and Marcus theory can be employed to study the CT process.[60] CT has been associated with the electron injection rate (Φ_{inject}) or efficiency which may be quantified by the free energy change for electron injection (ΔG_{inject}) in DSSCs, as described by the equation $J_{SC} = \int LHE(\lambda)\Phi_{inject}\eta_{collect}\, d\lambda$. The injection energy can be calculated as[65] $\Delta G_{inject} = E_{dye^*} - E_{CB}$, where E_{CB} is the reduction potential of the conduction band (CB) of the cluster, $Ti_{16}O_{34}$. E_{CB} corresponds to the LUMO energy (−3.53 eV) of the cluster. The oxidation potential of the excitation of the dye (E_{dye^*}) can be computed by subtracting the vertical transition energy (λ_{max}) from the redox potential of the ground state of the dye (E_{dye}) whereas $E_{dye} = -E_{HOMO}$, according to Koopmans' theorem. All the designed dyes show the negative values of ΔG_{inject}, which implies that the excited states of the

https://dx.doi.org/10.1021/acssuschemeng.0c04061
ACS Sustainable Chem. Eng. 2020, 8, 13328−13341

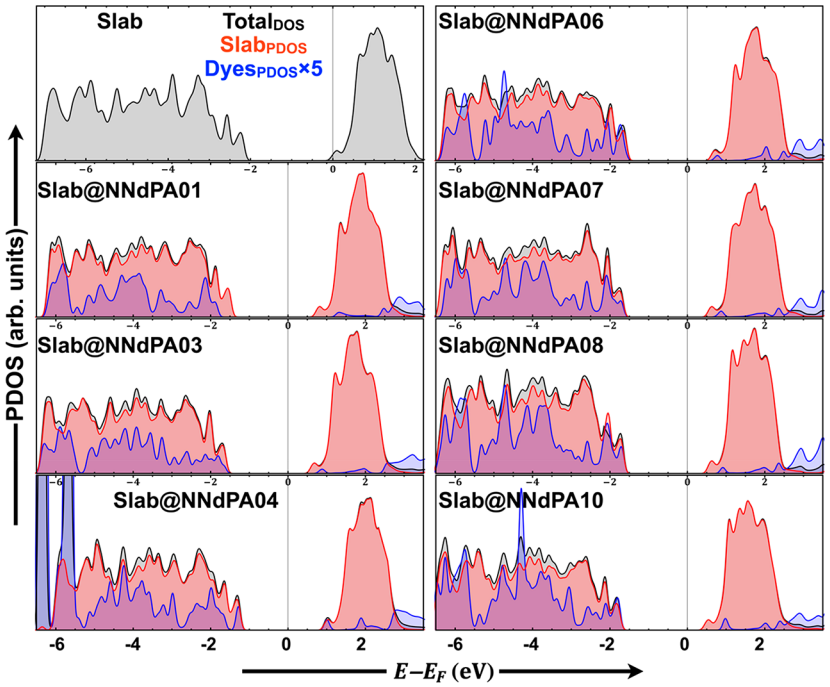

Figure 9. PDOS of the pristine slab and dyes@slab. PDOS of dyes is multiplied by 5 to magnify the effects near the conduction band minima (CBM) and valence band maxima (VBM) of TiO_2.

dyes lies above the CB edge of TiO_2 with an effective charge transfer excitation character.[66] The negative ΔG_{inject} values reported in Table 3 indicate that all the NNdPA dyes reveal spontaneity of the electron flow to the CB of TiO_2. The nature of the Fermi energy shift of TiO_2 after the adsorption dye also can be used to predict the efficient electron injection. Besides, we computed the Fermi level shift after the adsorption of different dyes on the cluster from the PDOS (Supporting Information Figure S4A). It provides clear evidence that the adsorbed dyes introduced new occupied states in the gap region of the cluster which shifts the Fermi or the HOMO energy (concerning clean TiO_2 DOS) toward the CB edge to make the electron injection more favorable.

We also computed the chemical reactivity (CR) parameters such as chemical hardness, electrophilicity and electron-donating and electron-accepting powers of the designed dyes (see Supporting Information for the calculation details and Table S3). Important CR parameters are plotted in Figure 5. Chemical hardness is a crucial factor that can resist the intramolecular charge transfer. NNdPA04 shows the lowest chemical hardness and highest electron-donating power which indicates that this dye would possess greater J_{SC} and hence higher PCE.[67] NNdPA06, NNdPA07, NNdPA08, and NNdPA10 display the same trends for all the chemical reactivity parameters. However, NNdPA01 reveals the highest chemical hardness with the electrophilicity and electron-accepting and -donating powers. The introduction of the coacceptor like BTD along with fused π-conjugation would improve the electron injection.

Open-Circuit Voltage. The V_{OC} is one of the salient features of the DSSCs that can be determined by the difference between the quasi-Fermi level of the sensitized TiO_2 semiconductor and the redox potential of I^-/I_3^-.[68]

$$V_{OC} = \frac{E_{CB} - E_{redox}}{q} + \frac{k_B T}{q} \ln\left(\frac{n_c}{N_{CB}}\right) \quad (10)$$

One can expect a variation in the band energy alignment of the dyes or cluster after the adsorption, as the result of the interaction between the orbitals of the surface of the semiconductor and dyes. The shift of the CB energy (ΔE_{CB}) of TiO_2 after dye adsorption can be approximated by the difference between the intercepts of the fitted lines of TiO_2 PDOS and pure TiO_2 DOS on the axis of energy Figure 6. All the dyes (see Figure S4B, Supporting Information) after adsorption on the TiO_2 surface shift the CB edge of TiO_2 toward the more positive direction concerning the pristine CB of TiO_2. The $E_{\Delta CB}$ provides the indirect evidence that allows predicting the V_{OC} for the fast screening of newly designed dyes. The trend of the CB shift is as follows: NNdPA10 (0.38 eV) > NNdPA04 (0.35 eV) > NNdPA08 (0.28 eV) > NNdPA06 (0.27 eV) > NNdPA07 (0.24 eV) > NNdPA03 (0.20 eV) > NNdPA01 (0.18 eV). All the dyes with fused π-conjugation along with the BTD unit largely shifted the TiO_2 CB edge toward the positive direction which implies the increase in V_{OC}. The bulky alkyl group in NNdPA10 would favor the V_{OC} by suppressing the charge recombination.

The charge recombination dynamics of the oxidized dye reduced the V_{OC} and accordingly the PCE. This undesirable recombination may occur by two routes either due to the (i) back electron transfer from the semiconductor to the dye molecules after electron injection or (ii) reduction of electrolytes by receiving an electron from the sensitizer rather than from the counter electrode.[69] We investigate the second routes of charge recombination by taking into account the halogen bond distances between iodine electrolytes and heteroatoms of sensitizers like sulfur and nitrogen atoms.[70] We considered three different configurations of the isolated dye···I_2 complex as shown in Figure 6b for NNdPA07 along with the three different additives. The lengths of CN···I and S···I together with the corresponding binding energies are tabulated in Table S5 in the Supporting Information.

https://dx.doi.org/10.1021/acssuschemeng.0c04061
ACS Sustainable Chem. Eng. 2020, 8, 13328−13341

The value of the CN···I bond length lies between 2.59 Å (NNdPA01 and NNdPA03) and 2.70 Å (NNdPA06). The bond length of the S···I halogen bond varies from 2.82 to 4.03 Å (NNdPA06). The binding energy of the halogen bonds is under −1.0 eV with the lowest 0.01 eV for NNdPA06. A more negative binding energy implies the stronger interaction and higher stability of the bonds. A larger bond length and the highest binding energy favor NNdPA06 by suppressing charge recombination. The additives used to reduce the iodine concentration in the vicinity of TiO_2 are *N*-methylbenzimidazole (NMBI), 2-methylquinoline (MQ), and 4-*t*-butylpyridine (TBP). The bond distances of the optimized additive−I_2 adducts are 2.34 Å, 2.45 Å, and 2.38 Å, respectively (smaller than those of the dye···I_2 complexes), indicating that the designed dyes could efficiently reduce the iodine concentration near the TiO_2 surface.

Besides, charge recombination is vital to applications of dye sensitizers with higher dye-regeneration efficiency to suppress the charge recombination. Dye regeneration efficiency can be estimated in terms of the driving force between the electrolyte and the oxidized dye by the following equation:

$$\Delta G_{Reg} = E^{Redox} - E_{GSOP} \quad (11)$$

where ΔG_{Reg}, E^{Redox}, and E_{GSOP} represent driving force of dye regeneration, the redox potential of the iodine electrolyte (−4.8 eV), and the ground state oxidation potential of the dyes, respectively. The values (Table 3) of ΔG_{Reg} for all the NNdPA dyes are higher than the ΔG_{Inject} value, confirming that the regeneration dynamics is more stable than electron injection.[71] The introduction of fused π-conjugation does not affect the regeneration efficiency of the NNdPA dyes.

Photostability of the Excited Dyes. The photostability is one of the most vital factors which infers the stability of the oxidized dyes and the duration of the DSSC devices. We applied a very fast and robust screening approach to identify the most photostable NNdPA dyes based on their aligned excited state energy (ESOP). Figure 7 depicts the GSOPs, ESOPs, and FMOs of dye@cluster complexes. Considering the size of the system, ESOP was computed from the ground state oxidation potential (GSOP) and vertical excitation energy. We estimated GSOP by the approximation: GSOP = $[E_{neutral} - E_{cation}]_{GS}$, and ESOP was predicted by the relation: ESOP ≅ GSOP − E_{Abs}, where E_{Abs} is the first excitation energy. It is noted that NNdPA04 has the relatively lowest driving force while NNdPA01 is characterized by the highest gradient to the CB edge of TiO_2. Excited state lifetimes (τ_e) also have a greater weight toward the long-term stability of the dye which facilitates the efficient charge transfer. Stable cationic forms with longer excited state lifetime are also important factors characterizing the charge transfer phenomenon. The τ_e values of the NNdPA dyes can be estimated by the $\tau_e = 1.499/fE^2$ relationship[72] where E is the excitation energy (cm^{-1}) of the lowest electronic state and f is the oscillator strength. The first excited state lifetimes of all the dyes are tabulated in Table 1. Relative τ_e follows the trend NNdPA04 > NNdPA03 > NNdPA10 > NNdPA07 > NNdPA08 > NNdPA01 > NNdPA06. The longest lifetime for NNdPA04 definitely ensures the efficient charge transfer, electron injection into the CB of TiO_2, and stability after electron injection. The introduction of a coacceptor like the BTD unit along with the effective conjugation unit (such as the number and nature of heteroatoms in the conjugation unit[39]) would improve the excited state lifetime of the NNdPA dyes. Excited state lifetimes, τ_e (Table 4), of NNdPA dyes are also in good agreement with the photostability. Due to the presence of the BTD unit as the coacceptor and planar fused π-conjugation with fewer heteroatoms, NNdPA04 is the most stable dye with the highest τ_e value. On the other hand, NNdPA06 shows the lowest τ_e value with large driving force and blue-shift in the ICT band (Table 1). Also, the HOMO and LUMO of the complexes of NNdPA04, NNdPA07, NNdPA08, and NNdPA10 are well distributed to the donor moieties and the interface of the complexes.

Emission Characteristics. Emission spectra of the designed NNdPA dyes were computed in the gas phase to reveal the kinetics of radiative and nonradiative decays of the excited state as the electron injection process governed the decays. The radiative lifetime of the fluorescence (τ_f) predicted by the relation[73] $\tau_f = c^3/(2 \times (E_{emi})^2 \times f)$, where c is the velocity of light and emission energies (E_{emi}) and oscillator strengths (f) are in au for the $S_0 \leftarrow S_1$ transition. The emission spectra and related computed fluorescence properties of the dyes are depicted in Figure 8 and Table 5, respectively. The result revealed that NNdPA04 showed the largest emission peak and Stokes shift among all designed dyes with the lowest τ_f.

Periodic DFT. We also investigated the adsorption behavior and electronic structure of the NNdPA dyes considering the anatase surface. The optimized structures of dye@slabs are depicted in Figure S5 (see Supporting Information). To get insight into the bonding interaction of the adsorbed dyes on the TiO_2 surface, we plotted the computed PDOS of dye@slabs in Figure 9. The band gap of the dye@slab complex is decreased in the case of all the NNdPA dyes. The conduction band minima (CBM) and valence band maxima (VBM) of the slab reveal a downward and an upward shift compared to the pristine slab, respectively. The downward shift of the CBM might reduce the value of V_{OC}. However, the location of the LUMO of the adsorbed dye under the CBM will expedite the electron injection. In Figure 8, one can observe that the VBM of the dye@slab changes due to the strong overlap between the DOS of the dyes and the valence band (VB) of the pristine slab. The substantial overlap indicates that the dyes introduce few π-occupied levels on the top of the TiO_2 VB. The newly introduced π-occupied levels become the top of the VBM. For the efficient electron injection, the LUMO of the adsorbed dyes should be under or on the CBM of the semiconductor. In our PDOS analysis, we observed that the energy level of the LUMO of all the adsorbed dyes is higher than the CBM of the semiconductor (except NNdPA04). In NNdPA04, the LUMO of the dye has a strong electronic coupling with the CBM of the surface, which will improve the electron injection process. It is evident that the insertion of the BTD moiety and fused π-spacer influence the position of the energy level of the LUMO of the adsorbed dyes.

CONCLUSIONS

In this work, novel D−D−π−A NNdPA-based dyes designed with two NNdPA donor units, fused π-conjugation as a conjugated bridge, and cyanoacrylic acid (CAA) as an acceptor along with a BTD unit as the coacceptor or π-spacer were evaluated. We carried out a systematic ground and excited state investigation on the photoelectric properties of the designed NNdPA dyes via DFT and TDDFT approaches. To elucidate the interface behavior of the dyes and TiO_2, we performed

https://dx.doi.org/10.1021/acssuschemeng.0c04061
ACS Sustainable Chem. Eng. 2020, 8, 13328−13341

cluster DFT and periodic DFT computations. Moreover, a detailed analysis revealed how the number and types of rings in the fused π-conjugation bridge could influence the electrochemical properties of the double donor sensitizer based DSSCs. The critical parameters related to J_{SC} and V_{OC} such as the driving force of electron injection (ΔG_{Inject}), the spontaneity of dye regeneration (ΔG_{Reg}), the exciton binding synergy (E_b), the CT length (d_{CT}), the reorganization energy (λ_{Total}), the shift of the CB of TiO_2 (ΔE_{CB}), and the chemical reactivity parameters were computed. The computed results implied that the fused π-conjugation bridge along with the BTD unit improves the absorption spectrum and charge separation d_{CT}. The location of the benzene ring at the donor side positively affects the electron transfer with lower λ_{Total}, balancing its counterpart's reorganization energy. Emission characteristics of the designed dyes were also predicted by gas phase calculations. NNdPA04 showed a promising largest Stokes shift with an acceptable radiative fluorescence lifetime.

It is evident that the fused π-conjugation bridge along with the BTD unit conducive to chemical reactivity parameters positively affects the J_{SC}. Considering the state after electron injection, NNdPA04 would possess the most stable excited state due to its longer excited state lifetime, τ_e, with the lowest driving force between ESOP and CBM of TiO_2. We found that the presence of the benzene ring in fused π-conjugation increases the light-harvesting by shifting the UV−vis spectrum to a longer wavelength. The value of ΔE_{CB} and ΔG_{Reg} suggests that the NNdPA04 and NNdPA10 would be able to suppress the charge recombination and thus enhance V_{OC} of the NNdPA-based dyes. Periodic DFT analysis revealed that the energy levels of the LUMOs of the adsorbed dyes are located under or on the CBM of TiO_2. By considering all the above factors, it is evident that the designed NNdPA04 should be the most preferable for the considered system. Our work also provides an insight into designing the D−D−π−A dyes with a fused π-spacer and furnishes enough details to assist the synthesis and applications of such sensitizers.

■ ASSOCIATED CONTENT

Supporting Information

The Supporting Information is available free of charge at https://pubs.acs.org/doi/10.1021/acssuschemeng.0c04061.

Additional optimized structures of isolated NNdPA dyes and dyes@TiO_2, energetics of FMOs of dyes including cationic, neutral, and single donor, Fermi level and CB shift, IP, EA, simulated UV−vis parameters, and dye−I_2 bond distances (PDF)

■ AUTHOR INFORMATION

Corresponding Author

Jerzy Leszczynski − *Interdisciplinary Center for Nanotoxicity, Department of Chemistry, Physics and Atmospheric Sciences, Jackson State University, Jackson, Mississippi 39217, United States;* orcid.org/0000-0001-5290-6136; Phone: +1 601 979 3723; Email: jerzy@icnanotox.org; Fax: +1 601 979 7823

Authors

Juganta K. Roy − *Interdisciplinary Center for Nanotoxicity, Department of Chemistry, Physics and Atmospheric Sciences, Jackson State University, Jackson, Mississippi 39217, United States;* orcid.org/0000-0002-3646-5593

Supratik Kar − *Interdisciplinary Center for Nanotoxicity, Department of Chemistry, Physics and Atmospheric Sciences, Jackson State University, Jackson, Mississippi 39217, United States;* orcid.org/0000-0002-9411-2091

Complete contact information is available at: https://pubs.acs.org/10.1021/acssuschemeng.0c04061

Notes

The authors declare no competing financial interest.

■ ACKNOWLEDGMENTS

The authors are thankful to the Department of Energy (Grant Number DE-SC0018322) and the NSF EPSCoR (Grant Number OIA-1757220) for financial support. We also would like to acknowledge the Extreme Science and Engineering Discovery Environment (XSEDE) by the National Science Foundation Grant Number OCI-1053575 and XSEDE Award Allocation Number DMR110088 and DMR110013P for providing state-of-the-art high-performance computing facilities for supporting this research.

■ REFERENCES

(1) REN21. *Renewables 2019 Global Status Report*; Paris, 2019.

(2) O'Regan, B.; Grätzel, M. A Low-Cost, High-Efficiency Solar Cell Based on Dye-Sensitized Colloidal TiO2 Films. *Nature* **1991**, *353*, 737−740.

(3) Nusbaumer, H.; Zakeeruddin, S. M.; Moser, J.-E.; Grätzel, M. An Alternative Efficient Redox Couple for the Dye-Sensitized Solar Cell System. *Chem. - Eur. J.* **2003**, *9*, 3756−3763.

(4) Zhang, L.; Yang, X.; Wang, W. G.; Gurzadyan, G.; Li, J.; Li, X.; An, J.; Yu, Z.; Wang, H.; Cai, B.; Hagfeldt, A.; Sun, L. 13.6% Efficient Organic Dye-Sensitized Solar Cells by Minimizing Energy Losses of the Excited State. *ACS Energy Lett.* **2019**, *4* (4), 943−951.

(5) Mishra, A.; Fischer, M. K. R.; Bäuerle, P. Metal-Free Organic Dyes for Dye-Sensitized Solar Cells: From Structure: Property Relationships to Design Rules. *Angew. Chem., Int. Ed.* **2009**, *48*, 2474−2499.

(6) Liang, M.; Chen, J. Arylamine Organic Dyes for Dye-Sensitized Solar Cells. *Chem. Soc. Rev.* **2013**, *42* (8), 3453.

(7) Shibayama, N.; Inoue, Y.; Abe, M.; Kajiyama, S.; Ozawa, H.; Miura, H.; Arakawa, H. Novel Near-Infrared Carboxylated 1,3-Indandione Sensitizers for Highly Efficient Flexible Dye-Sensitized Solar Cells. *Chem. Commun.* **2015**, *51* (64), 12795−12798.

(8) Qian, X.; Zhu, Y.-Z.; Chang, W.-Y.; Song, J.; Pan, B.; Lu, L.; Gao, H.-H.; Zheng, J.-Y. Benzo[*a*]Carbazole-Based Donor-π-Acceptor Type Organic Dyes for Highly Efficient Dye-Sensitized Solar Cells. *ACS Appl. Mater. Interfaces* **2015**, *7* (17), 9015−9022.

(9) Cai, N.; Li, R.; Wang, Y.; Zhang, M.; Wang, P. Organic Dye-Sensitized Solar Cells with a Cobalt Redox Couple: Influences of π-Linker Rigidification and Dye-Bath Solvent Selection. *Energy Environ. Sci.* **2013**, *6* (1), 139−147.

(10) Haid, S.; Marszalek, M.; Mishra, A.; Wielopolski, M.; Teuscher, J.; Moser, J. E.; Humphry-Baker, R.; Zakeeruddin, S. M.; Grätzel, M.; Bäuerle, P. Significant Improvement of Dye-Sensitized Solar Cell Performance by Small Structural Modification in π-Conjugated Donor-Acceptor Dyes. *Adv. Funct. Mater.* **2012**, *22* (6), 1291−1302.

(11) Kar, S.; Roy, J.; Leszczynska, D.; Leszczynski, J. Power Conversion Efficiency of Arylamine Organic Dyes for Dye-Sensitized Solar Cells (DSSCs) Explicit to Cobalt Electrolyte: Understanding the Structural Attributes Using a Direct QSPR Approach. *Computation* **2017**, *5* (4), 2.

(12) Aono, C. M.; Coutinho-Neto, M.; Miotto, R.; Homem-De-Mello, P. CAHM1: A Theory-Based Proposal for a New DSSC D-A-π-A Dye. *J. Phys. Chem. C* **2018**, *122* (48), 27256−27262.

(13) Grisorio, R.; De Marco, L.; Baldisserri, C.; Martina, F.; Serantoni, M.; Gigli, G.; Suranna, G. P. Sustainability of Organic Dye-

Sensitized Solar Cells: The Role of Chemical Synthesis. *ACS Sustainable Chem. Eng.* **2015**, *3* (4), 770−777.
(14) Hong, Y.; Liao, J.-Y.; Cao, D.; Zang, X.; Kuang, D.-B.; Wang, L.; Meier, H.; Su, C.-Y. Organic Dye Bearing Asymmetric Double Donor-π-Acceptor Chains for Dye-Sensitized Solar Cells. *J. Org. Chem.* **2011**, *76* (19), 8015−8021.
(15) Hagberg, D. P.; Yum, J. H.; Lee, H. J.; De Angelis, F.; Marinado, T.; Karlsson, K. M.; Humphry-Baker, R.; Sun, L.; Hagfeldt, A.; Grätzel, M.; Nazeeruddin, M. K. Molecular Engineering of Organic Sensitizers for Dye-Sensitized Solar Cell Applications. *J. Am. Chem. Soc.* **2008**, *130* (19), 6259−6266.
(16) Capodilupo, A. L.; De Marco, L.; Corrente, G. A.; Giannuzzi, R.; Fabiano, E.; Cardone, A.; Gigli, G.; Ciccarella, G. Synthesis and Characterization of a New Series of Dibenzofulvene Based Organic Dyes for DSSCs. *Dyes Pigm.* **2016**, *130*, 79−89.
(17) Namuangruk, S.; Fukuda, R.; Ehara, M.; Meeprasert, J.; Khanasa, T.; Morada, S.; Kaewin, T.; Jungsuttiwong, S.; Sudyoadsuk, T.; Promarak, V. D-D-π-A-Type Organic Dyes for Dye-Sensitized Solar Cells with a Potential for Direct Electron Injection and a High Extinction Coefficient: Synthesis, Characterization, and Theoretical Investigation. *J. Phys. Chem. C* **2012**, *116* (49), 25653−25663.
(18) Sharmoukh, W.; Cong, J.; Gao, J.; Liu, P.; Daniel, Q.; Kloo, L. Molecular Engineering of D-D-π-A-Based Organic Sensitizers for Enhanced Dye-Sensitized Solar Cell Performance. *ACS Omega* **2018**, *3* (4), 3819−3829.
(19) Jiang, S.; Chen, Y.; Li, Y.; Han, L. Novel D-D-π-A Indoline-Linked Coumarin Sensitizers for Dye-Sensitized Solar Cells. *J. Photochem. Photobiol., A* **2019**, *384*, 112031.
(20) Estrella, L. L.; Balanay, M. P.; Kim, D. H. Theoretical Insights into D-D-π-A Sensitizers Employing N-Annulated Perylene for Dye-Sensitized Solar Cells. *J. Phys. Chem. A* **2018**, *122* (30), 6328−6342.
(21) Murakami, T. N.; Koumura, N.; Kimura, M.; Mori, S. Structural Effect of Donor in Organic Dye on Recombination in Dye-Sensitized Solar Cells with Cobalt Complex Electrolyte. *Langmuir* **2014**, *30* (8), 2274−2279.
(22) Li, Y.; Sun, C.; Song, P.; Ma, F.; Yang, Y. Tuning the Electron-Transport and Electron-Accepting Abilities of Dyes through Introduction of Different π-Conjugated Bridges and Acceptors for Dye-Sensitized Solar Cells. *ChemPhysChem* **2017**, *18* (4), 366−383.
(23) Ni, J.-S.; Yen, Y.-C.; Lin, J. T. Organic Dyes with a Fused Segment Comprising Benzotriazole and Thieno[3{,}2-b]Pyrrole Entities as the Conjugated Spacer for High Performance Dye-Sensitized Solar Cells. *Chem. Commun.* **2015**, *51* (96), 17080−17083.
(24) Baumann, A.; Watson, J.; Delcamp, J. H. Robust, Scalable Synthesis of the Bulky Hagfeldt Donor for Dye-Sensitized Solar Cells. *ChemSusChem* **2020**, *13*, 283.
(25) Li, Y.; Sun, C.; Song, P.; Ma, F.; Kungwan, N.; Sun, M. Physical Insight on Mechanism of Photoinduced Charge Transfer in Multipolar Photoactive Molecules. *Sci. Rep.* **2018**, *8* (1), 10089.
(26) Kar, S.; Roy, J. K.; Leszczynski, J. In Silico Designing of Power Conversion Efficient Organic Lead Dyes for Solar Cells Using Todays Innovative Approaches to Assure Renewable Energy for Future. *npj Comput. Mater.* **2017**, *3* (1), 22.
(27) Berardo, E.; Kaplan, F.; Bhaskaran-Nair, K.; Shelton, W. A.; van Setten, M. J.; Kowalski, K.; Zwijnenburg, M. A. Benchmarking the Fundamental Electronic Properties of Small TiO_2 Nanoclusters by *GW* and Coupled Cluster Theory Calculations. *J. Chem. Theory Comput.* **2017**, *13* (8), 3814−3828.
(28) Berardo, E.; Hu, H.-S.; van Dam, H. J. J.; Shevlin, S. A.; Woodley, S. M.; Kowalski, K.; Zwijnenburg, M. A. Describing Excited State Relaxation and Localization in TiO_2 Nanoparticles Using TD-DFT. *J. Chem. Theory Comput.* **2014**, *10* (12), 5538−5548.
(29) Li, P.; Cui, Y.; Song, C.; Zhang, H. A Systematic Study of Phenoxazine-Based Organic Sensitizers for Solar Cells. *Dyes Pigm.* **2017**, *137*, 12−23.
(30) Fan, W.-J.; Shi, H.; Tan, D.-Z.; Xu, Z.-N.; Yu, N.-K.; Zhao, J.-L. Design of Novel Phenanthrocarbazole Dyes for Efficient Applications in Dye-Sensitized Solar Cells. *Comput. Mater. Sci.* **2018**, *151*, 34−40.
(31) Ding, W.-L.; Wang, D.-M.; Geng, Z.-Y.; Zhao, X.-L.; Yan, Y.-F. Molecular Engineering of Indoline-Based D-A-π-A Organic Sensitizers toward High Efficiency Performance from First-Principles Calculations. *J. Phys. Chem. C* **2013**, *117* (34), 17382−17398.
(32) Zhang, W.; Heng, P.; Su, H.; Ren, T.; Wang, L.; Zhang, J. Rational Design of High-Efficiency Organic Dyes in Dye-Sensitized Solar Cells by Multiscale Simulations. *J. Phys. Chem. C* **2018**, *122* (44), 25219−25228.
(33) Chiu, C.-C.; Sheng, Y.-C.; Lin, W.-J.; Juwita, R.; Tan, C.-J.; Tsai, H.-H. G. Effects of Internal Electron-Withdrawing Moieties in D-A-π-A Organic Sensitizers on Photophysical Properties for DSSCs: A Computational Study. *ACS Omega* **2018**, *3* (1), 433−445.
(34) Roy, J. K.; Kar, S.; Leszczynski, J. Electronic Structure and Optical Properties of Designed Photo-Efficient Indoline-Based Dye-Sensitizers with D-A-π-A Framework. *J. Phys. Chem. C* **2019**, *123* (6), 3309−3320.
(35) Grätzel, M. Recent Advances in Sensitized Mesoscopic Solar Cells. *Acc. Chem. Res.* **2009**, *42* (11), 1788−1798.
(36) Katoh, R.; Furube, A.; Yoshihara, T.; Hara, K.; Fujihashi, G.; Takano, S.; Murata, S.; Arakawa, H.; Tachiya, M. Efficiencies of Electron Injection from Excited N3 Dye into Nanocrystalline Semiconductor (ZrO 2, TiO 2, ZnO, Nb 2 O 5, SnO 2, In 2 O 3) Films. *J. Phys. Chem. B* **2004**, *108* (15), 4818−4822.
(37) Frisch, M. J.; Trucks, G. W.; Schlegel, H. B.; Scuseria, G. E.; Robb, M. A.; Cheeseman, J. R.; Scalmani, G.; Barone, V.; Mennucci, B.; Petersson, G. A.; Nakatsuji, H.; Caricato, M.; Li, X.; Hratchian, H. P.; Izmaylov, A. F.; Bloino, J.; Zheng, G.; Sonnenberg, J. L.; Hada, M.; Ehara, M.; Toyota, K.; Fukuda, R.; Hasegawa, J.; Ishida, M.; Nakajima, T.; Honda, Y.; Kitao, O.; Nakai, H.; Vreven, T.; Montgomery, J. A., Jr.; Peralta, J. E.; Ogliaro, F.; Bearpark, M.; Heyd, J. J.; Brothers, E.; Kudin, K. N.; Staroverov, V. N.; Kobayashi, R.; Normand, J.; Raghavachari, K.; Rendell, A.; Burant, J. C.; Iyengar, S. S.; Tomasi, J.; Cossi, M.; Rega, N.; Millam, J. M.; Klene, M.; Knox, J. E.; Cross, J. B.; Bakken, V.; Adamo, C.; Jaramillo, J.; Gomperts, R.; Stratmann, R. E.; Yazyev, O.; Austin, A. J.; Cammi, R.; Pomelli, C.; Ochterski, J. W.; Martin, R. L.; Morokuma, K.; Zakrzewski, V. G.; Voth, G. A.; Salvador, P.; Dannenberg, J. J.; Dapprich, S.; Daniels, A. D.; Farkas, Ö.; Foresman, J. B.; Ortiz, J. V.; Cioslowski, J.; Fox, D. J. *Gaussian 09*, revision E.01; Gaussian, Inc.: Wallingford, CT, 2013.
(38) Lu, T.; Chen, F. Multiwfn: A Multifunctional Wavefunction Analyzer. *J. Comput. Chem.* **2012**, *33* (5), 580−592.
(39) Yang, Z.; Liu, C.; Li, K.; Cole, J. M.; Shao, C.; Cao, D. Rational Design of Dithienopicenocarbazole-Based Dyes and a Prediction of Their Energy-Conversion Efficiency Characteristics for Dye-Sensitized Solar Cells. *ACS Appl. Energy Mater.* **2018**, *1* (4), 1435−1444.
(40) Hagfeldt, A.; Boschloo, G.; Sun, L.; Kloo, L.; Pettersson, H. Dye-Sensitized Solar Cells. *Chem. Rev.* **2010**, *110* (11), 6595−6663.
(41) Kresse, G.; Hafner, J. Ab Initio Molecular Dynamics for Liquid Metals. *Phys. Rev. B: Condens. Matter Mater. Phys.* **1993**, *47* (1), 558−561.
(42) Kresse, G.; Hafner, J. Ab Initio Molecular-Dynamics Simulation of the Liquid-Metal-Amorphous-Semiconductor Transition in Germanium. *Phys. Rev. B: Condens. Matter Mater. Phys.* **1994**, *49* (20), 14251−14269.
(43) Kresse, G.; Furthmüller, J. Efficiency of Ab-Initio Total Energy Calculations for Metals and Semiconductors Using a Plane-Wave Basis Set. *Comput. Mater. Sci.* **1996**, *6* (1), 15−50.
(44) Hubbard, J. Electron Correlations in Narrow Energy Bands. *Proc. R. Soc. London A Math. Phys. Eng. Sci.* **1963**, *276* (1365), 238−257.
(45) Roy, J. K.; Kar, S.; Leszczynski, J. Insight into the Optoelectronic Properties of Designed Solar Cells Efficient Tetrahydroquinoline Dye-Sensitizers on TiO2(101) Surface: First Principles Approach. *Sci. Rep.* **2018**, *8*, 10997.
(46) Kresse, G.; Joubert, D. From Ultrasoft Pseudopotentials to the Projector Augmented-Wave Method. *Phys. Rev. B: Condens. Matter Mater. Phys.* **1999**, *59* (3), 1758−1775.
(47) Liu, H.; Li, B.; Xue, B.; Liu, E. Theoretical Design of High-Performance Boron Dipyrromethenes Dyes by Introducing Hetero-

https://dx.doi.org/10.1021/acssuschemeng.0c04061
ACS Sustainable Chem. Eng. 2020, 8, 13328−13341

cyclics to Tune Photoelectric Properties. *J. Phys. Chem. C* **2019**, *123* (43), 26047−26056.
(48) Yasuda, T.; Shinohara, Y.; Matsuda, T.; Han, L.; Ishi-I, T. Improved Power Conversion Efficiency of Bulk-Heterojunction Organic Solar Cells Using a Benzothiadiazole-Triphenylamine Polymer. *J. Mater. Chem.* **2012**, *22* (6), 2539−2544.
(49) Chou, H. H.; Chen, Y. C.; Huang, H. J.; Lee, T. H.; Lin, J. T.; Tsai, C.; Chen, K. High-Performance Dye-Sensitized Solar Cells Based on 5,6-Bis-Hexyloxy- Benzo[2,1,3]Thiadiazole. *J. Mater. Chem.* **2012**, *22* (21), 10929−10938.
(50) Kim, J.; Kwon, Y. S.; Shin, W. S.; Moon, S.-J.; Park, T. Carbazole-Based Copolymers: Effects of Conjugation Breaks and Steric Hindrance. *Macromolecules* **2011**, *44* (7), 1909−1919.
(51) Lin, R. Y.-Y.; Lee, C.-P.; Chen, Y.-C.; Peng, J.-D.; Chu, T.-C.; Chou, H.-H.; Yang, H.-M.; Lin, J. T.; Ho, K.-C. Benzothiadiazole-Containing Donor-Acceptor-Acceptor Type Organic Sensitizers for Solar Cells with ZnO Photoanodes. *Chem. Commun.* **2012**, *48* (99), 12071−12073.
(52) Kumar, D.; Thomas, K. R. J.; Lee, C.-P.; Ho, K.-C. Novel Pyrenoimidazole-Based Organic Dyes for Dye-Sensitized Solar Cells. *Org. Lett.* **2011**, *13* (10), 2622−2625.
(53) Pastore, M.; De Angelis, F. Aggregation of Organic Dyes on TiO2 in Dye-Sensitized Solar Cells Models: An Ab Initio Investigation. *ACS Nano* **2010**, *4* (1), 556−562.
(54) Chen, P.; Yum, J. H.; Angelis, F. De; Mosconi, E.; Fantacci, S.; Moon, S.-J.; Baker, R. H.; Ko, J.; Nazeeruddin, M. K.; Grätzel, M. High Open-Circuit Voltage Solid-State Dye-Sensitized Solar Cells with Organic Dye. *Nano Lett.* **2009**, *9* (6), 2487−2492.
(55) Martsinovich, N.; Troisi, A. Theoretical Studies of Dye-Sensitised Solar Cells: From Electronic Structure to Elementary Processes. *Energy Environ. Sci.* **2011**, *4* (11), 4473.
(56) Jacquemin, D.; Bahers, T. Le; Adamo, C.; Ciofini, I. What Is the "Best" Atomic Charge Model to Describe through-Space Charge-Transfer Excitations? *Phys. Chem. Chem. Phys.* **2012**, *14* (16), 5383.
(57) Le Bahers, T.; Adamo, C.; Ciofini, I. A Qualitative Index of Spatial Extent in Charge-Transfer Excitations. *J. Chem. Theory Comput.* **2011**, *7* (8), 2498−2506.
(58) Gregg, B. A. Excitonic Solar Cells. *J. Phys. Chem. B* **2003**, *107*, 4688−4698.
(59) Scholes, G. D.; Rumbles, G. Excitons in Nanoscale Systems: Fundamentals and Applications. *Annu. Rev. Nano Res.* **2008**, *2*, 103−157.
(60) Marcus, R. A. R. Electron Transfer Reactions in Chemistry. Theory and Experiment. *J. Electroanal. Chem.* **1997**, *438* (1−2), 251−259.
(61) Hutchison, G. R.; Ratner, M. A.; Marks, T. J. Hopping Transport in Conductive Heterocyclic Oligomers: Reorganization Energies and Substituent Effects. *J. Am. Chem. Soc.* **2005**, *127* (7), 2339−2350.
(62) Shi, X.; Yang, Y.; Wang, L.; Li, Y. Introducing Asymmetry Induced by Benzene Substitution in a Rigid Fused π Spacer of D-π-A-Type Solar Cells: A Computational Investigation. *J. Phys. Chem. C* **2019**, *123* (7), 4007−4021.
(63) Marinado, T.; Hagberg, D. P.; Hedlund, M.; Edvinsson, T.; Johansson, E. M. J.; Boschloo, G.; Rensmo, H.; Brinck, T.; Sun, L.; Hagfeldt, A. Rhodanine Dyes for Dye-Sensitized Solar Cells: Spectroscopy{,} Energy Levels and Photovoltaic Performance. *Phys. Chem. Chem. Phys.* **2009**, *11* (1), 133−141.
(64) Zhang, Z.-L.; Zou, L.-Y.; Ren, A.-M.; Liu, Y.-F.; Feng, J.-K.; Sun, C.-C. Theoretical Studies on the Electronic Structures and Optical Properties of Star-Shaped Triazatruxene/Heterofluorene Co-Polymers. *Dyes Pigm.* **2013**, *96* (2), 349−363.
(65) Katoh, R.; Furube, A. Electron Injection Efficiency in Dye-Sensitized Solar Cells. *J. Photochem. Photobiol., C* **2014**, *20*, 1−16.
(66) Mendizabal, F.; Mera-Adasme, R.; Xu, W.-H.; Sundholm, D. Electronic and Optical Properties of Metalloporphyrins of Zinc on TiO2 Cluster in Dye-Sensitized Solar-Cells (DSSC). A Quantum Chemistry Study. *RSC Adv.* **2017**, *7* (68), 42677−42684.
(67) Soto-Rojo, R.; Baldenebro-López, J.; Glossman-Mitnik, D. Study of Chemical Reactivity in Relation to Experimental Parameters of Efficiency in Coumarin Derivatives for Dye Sensitized Solar Cells Using DFT. *Phys. Chem. Chem. Phys.* **2015**, *17* (21), 14122−14129.
(68) Marinado, T.; Nonomura, K.; Nissfolk, J.; Karlsson, M. K.; Hagberg, D. P.; Sun, L.; Mori, S.; Hagfeldt, A. How the Nature of Triphenylamine-Polyene Dyes in Dye-Sensitized Solar Cells Affects the Open-Circuit Voltage and Electron Lifetimes. *Langmuir* **2010**, *26* (4), 2592−2598.
(69) Raga, S. R.; Barea, E. M.; Fabregat-Santiago, F. Analysis of the Origin of Open Circuit Voltage in Dye Solar Cells. *J. Phys. Chem. Lett.* **2012**, *3* (12), 1629−1634.
(70) Richards, C. E.; Anderson, A. Y.; Martiniani, S.; Law, C.; O'Regan, B. C. The Mechanism of Iodine Reduction by TiO2 Electrons and the Kinetics of Recombination in Dye-Sensitized Solar Cells. *J. Phys. Chem. Lett.* **2012**, *3* (15), 1980−1984.
(71) Daeneke, T.; Mozer, A. J.; Uemura, Y.; Makuta, S.; Fekete, M.; Tachibana, Y.; Koumura, N.; Bach, U.; Spiccia, L. Dye Regeneration Kinetics in Dye-Sensitized Solar Cells. *J. Am. Chem. Soc.* **2012**, *134* (41), 16925−16928.
(72) Chaitanya, K.; Ju, X.-H.; Heron, B. M. Theoretical Study on the Light Harvesting Efficiency of Zinc Porphyrin Sensitizers for DSSCs. *RSC Adv.* **2014**, *4* (51), 26621−26634.
(73) Litani-Barzilai, I.; Bulatov, V.; Gridin, V. V.; Schechter, I. Detector Based on Time-Resolved Ion-Induced Voltage in Laser Multiphoton Ionization and Laser-Induced Fluorescence. *Anal. Chim. Acta* **2004**, *501* (2), 151−156.

NOTE ADDED AFTER ASAP PUBLICATION

This paper was published ASAP on August 24, 2020. Minor changes were made to text in Results and Discussion section. The revised paper was reposted on August 25, 2020.

https://dx.doi.org/10.1021/acssuschemeng.0c04061
ACS Sustainable Chem. Eng. 2020, 8, 13328−13341